Clays Clay Miner. (2023) 71:673–683
https://doi.org/10.1007/s42860-023-00263-3

ORIGINAL PAPER

Determination of Hansen Solubility Parameters of Raw Muscovite

Ming Weng · Xiuhua Wang

Accepted: 21 November 2023 / Published online: 12 December 2023

Abstract Muscovite has been used increasingly as a substrate in flexible electronics and fillers in high-performance nanocomposites. Muscovite-based interfacial interactions play a crucial rule in material fabrication. Hansen solubility parameters (HSPs) have proven useful in characterizing molecular interactions within/between condensed phases. The present study aimed to determine the HSPs of raw muscovite (RM) and to investigate solvent dispersion mechanisms of RM. To achieve this, the solubilities of RM in 17 solvents were evaluated by dispersion tests, and the HSPs of RM were calculated as the center of the optimal solubility rotated-ellipsoid in HSP space, which included all good solvents, had the smallest number of outliers, and had the smallest volume. The resulting dispersion, polar, and hydrogen bonding components of RM were 18.301, 2.366, and 3.727 $MPa^{1/2}$, respectively. By considering the HSPs and Kamlet-Taft's solvatochromic parameters of solvents, we concluded that the low polarity of RM is due to hindered K^+/H^+ exchange on the RM surface, resulting from limited water/moisture contact. For solvent dispersion of RM, essential conditions include strong dispersion forces and weak polar forces, finely tuned to match the surface property of RM at a certain hydration level. The HSPs of RM determined from dispersion tests were restricted to predicting/characterizing RM-based interfacial phenomena in an environment with strictly controlled water/moisture content. The HSP calculation method proposed herein was applicable to any clay mineral.

Keywords Dispersion · Hansen solubility parameters · Muscovite · Solubility rotated-ellipsoid

Associate Editor: Luyi Sun

M. Weng
College of Textile Science and Engineering (International Institute of Silk), Zhejiang Sci-Tech University, Hangzhou, Zhejiang 310018, People's Republic of China

X. Wang (✉)
National & Local United Engineering Laboratory for Textile Fiber Materials and Processing Technology, Zhejiang Sci-Tech University, Hangzhou, Zhejiang 310018, People's Republic of China
e-mail: wxiuhua@126.com

Introduction

Muscovite, a phyllosilicate with the formula $KAl_2(Si_3Al)O_{10}(OH)_2$, consists of an octahedral sheet sandwiched by two opposing tetrahedral sheets and interlayer K^+ ions to bond together the stack of 2:1 layers (Pauling, 1930). This structure facilitates cleavage along the (001) basal plane into thin flakes with atomic-level flatness (Pauling, 1930). Besides abundant reserves and low cost, muscovite possesses outstanding properties of strength, flexibility, optical transmittance, heat conduction, electric insulation, thermal stability, and chemical inertness (Yen et al., 2019). Increasing attention has been paid to

using 2D muscovite as substrates in flexible electronics (Yen et al., 2019; Zhong & Li, 2020) and fillers in high-performance nanocomposites (Arias et al., 2019; Mohammadi & Moghbeli, 2018; Zhang et al., 2022; Zhao et al., 2022). In the case of flexible electronics, thin films of inorganic electronic materials (e.g. oxide, metals, halides, chalcogenides, etc.) are formed on the freshly cleaved muscovite surfaces via van der Waals epitaxy; in the case of nanocomposites, muscovite nanoparticles are embedded into polymer matrixes to improve the mechanical, thermal, electrical, or impact properties of composites. In these applications, the molecular interactions at muscovite-based interfaces play a crucial role in controlling the morphology, structure, and properties of fabricated materials.

Hansen solubility parameters (HSPs) measure the strength of nonpolar and polar molecular interactions within or between condensed phases (Hansen, 1967). They are defined as:

$$\delta_d = \sqrt{\frac{E_d}{V}}, \delta_p = \sqrt{\frac{E_p}{V}}, \delta_h = \sqrt{\frac{E_h}{V}} \quad (1)$$

where subscripts d, p, and h denote dispersion, polar, and hydrogen bonding (HB) interactions, respectively; E denotes cohesive energy; and V denotes molar volume of the solvent in the liquid state.

The total or Hildebrand solubility parameter (Hildebrand, 1949), δ_t, is calculated as follows:

$$\delta_t = \sqrt{\delta_d^2 + \delta_p^2 + \delta_h^2} \quad (2)$$

The distance between the solubility parameters of phases m and n is defined as $\Delta\delta = \sqrt{\sum_i^{dim} \left(\delta_{n,i} - \delta_{m,i}\right)^2}$, where *dim* is the dimension of the solubility parameter system. Thermodynamically, a sufficiently small $\Delta\delta$ leads to a negative free energy of mixing and consequently to spontaneous mixing. This is the basic assumption in the application of HSPs.

In practice, HSPs were first used to select solvents for coatings and later extended to predict miscibility of solvents, compatibility of polymers, etc., and to characterize the surfaces of pigments, fibers, and fillers (Hansen, 1967, 2007). More recently, HSPs have been applied to guide the design and processing of nanocomposites composed of polymers and clay minerals (Qin et al., 2019). As reported, HSPs explain the behavior of clay minerals in physical processes such as dispersion in liquids (e.g. solvents and monomers) (Alin et al., 2015; Ho & Glinka, 2003) and basal spacing expansion (Choi et al., 2004) or exfoliation (Zhou et al., 2020) in solvents or polymers. HSPs also showed potential in identifying the optimal media for modifying the surfaces of clay minerals (Asgari & Sundararaj, 2018).

In other studies, the HSPs of clay minerals were determined: (1) to be the center of a solubility region in HSP space by solving an optimization problem based on the HSPs of solvents and clay solubilities therein (Hansen, 2007); (2) to be weighted averages of the HSPs of solvents and clay concentrations therein (Zhou et al., 2020); and (3) by a group-contribution method from parameters of partial or all chemical compounds of the clay mineral or a surfactant on its surface (Alin et al., 2015). When using the last method, approximations were involved inevitably when replacing specific groups, e.g. siloxane groups (–Si–O–Si–) in clay minerals or surfactants and quaternary ammonium ions ($R_4N^+X^-$) in surfactants, with chemical groups having known parameters. This may cause the predicted compatibility to deviate from observed fact (Hojiyev et al., 2017). The reported HSPs of raw clay minerals are rare (Table 1). Zhou et al. (2020) calculated the HSPs of raw halloysite and indicated that the dispersion of halloysite depended mainly on the polar, δ_p, and HB, δ_h, HSP components of solvents. Similar phenomena were observed by Choi et al. (2004) in the dispersion and basal spacing expansion of raw montmorillonite (Mnt); however, the HSPs values were not calculated. Surface modifications are commonly adopted to adjust the HSPs of clay minerals, and hence alter their dispersion abilities in solvents or polymers (Hojiyev et al., 2017; Huth et al., 2018) (Table 1). For instance, in contrast to the findings of Choi et al. (2004), the dispersion HSP component, δ_d, of solvents becomes predominant in and governs the dispersion of organophilic modified Mnt (Ho & Glinka, 2003; Huth et al., 2018). As far as the present authors are aware, the HSPs of natural mica, whether unmodified or modified, have not been addressed to date.

The present study, therefore, aimed to investigate the dispersion behavior of raw muscovite (RM) in 17 solvents having diverse polarities, and to propose a method for determining the HSPs of RM. A further objective was to explore the solvent-dispersion mechanisms of RM by a comprehensive examination of the HSPs and Kamlet-Taft's solvatochromic parameters of solvents.

https://doi.org/10.1007/s42860-023-00263-3 Published online by Cambridge University Press

Table 1 HSPs of clay minerals ($MPa^{1/2}$)

Material	Description	δ_t	δ_d	δ_p	δ_h	ref
Halloysite[a]	natural halloysite	27.3	16.8	12.6	17.4	Zhou et al. (2020)
Somasif MEE[a]	synthetic mica modified by a quaternary ammonium ion with poly(ethylene glycol) chains	18.51	17.9	2.8	3.5	Huth et al. (2018)
Somasif MTE[a]	synthetic mica modified by a quaternary ammonium ion with tri-octyl chains	18.68	17.8	3.6	4.3	Huth et al. (2018)
Somasif MAE[a]	synthetic mica modified by a quaternary ammonium ion consists mainly of two hydrogenated tails with a distribution of chain length (~65% C_{18}; ~30% C_{16}; ~5% C_{14})	18.70	17.7	3.6	4.9	Huth et al. (2018)
Somasif S-2HT-75[a]	synthetic mica modified by a quaternary ammonium ion consists mainly of two hydrogenated tails (C_{18} and C_{16})	18.84	17.6	4.0	5.5	Huth et al. (2018)
PVP-Mnt[b]	natural montmorillonite (Mnt) modified by poly(vinyl pyrrolidone)	24.27	18.8	13.4	7.5	Li et al. (2014)
PEG-Mnt[b]	natural Mnt modified by polyethylene glycol	28.15	22.2	11.2	13.2	Hansen (2007)
Cloisite 30B[b]	natural Mnt modified by methyl tallow bis-2-hydroxyethyl quaternary ammonium chloride	20.38	16.68	9.48	6.87	Lu et al. (2004)
HDTMA-Mnt[b]	natural Mnt modified by hexadecyltrimethyl ammonium	15.91	15.23	0	4.61	Hojiyev et al. (2017)
HDTPh-Mnt[b]	natural Mnt modified by hexadecyltriphenyl phosphonium bromide	17.91	17.91	0.4	0	Hojiyev et al. (2017)
Etho-Mnt[b]	natural Mnt modified by Ethoquad C-12	19.76	15.8	2	11.7	Hojiyev et al. (2017)
CPB-Mnt[b]	natural Mnt modified by cetylpyridinium bromide	16.84	16.25	2.29	3.78	Hojiyev et al. (2017)
2HT-75[b]	surfactant Arquad 2HT-75	17.62	17.4	1.3	2.9	Huth et al. (2018)

[a] HSPs determined by method 2

[b] HSPs determined by method 3

Experimental

Materials and methods

RM nanoparticles were purchased from Lingshou County Dongxin Mineral Products Processing Plant (Shijiazhuang, China). Organic solvents of analytical reagent grade, i.e. n,n-dimethyl acetamide, tetrahydrofuran, chloro-benzene, o-xylene, n-methyl-2-pyrrolidone, and ethyl benzoate were obtained from Shanghai Aladdin Biochemical Technology Co. Ltd. (Shanghai, China). Dimethyl sulfoxide, styrene (containing 10–15 ppm 4-tert-butylcatechol stabilizer), and 1,1,2,2-tetrachloroethane were obtained from Shanghai Macklin Biochemical Co. Ltd. (Shanghai, China). Acetonitrile, chloroform, n-heptane, ethanol, t-butyl alcohol, diethylene glycol, and ethyl acetate were obtained from Hangzhou Gaojing Fine Chemical Research Institute (Hangzhou, China). All solvents were used as received without further purification. Deionized water was self-made on site in the laboratory. The HSPs (Hansen, 2007) and Kamlet-Taft's solvatochromic parameters (Marcus, 1993) of the solvents tested are listed in Table 2.

Characterization

The spectrum of mica was measured using a Nicolet iS50 Fourier-transform infrared (FTIR) spectrometer (Thermo Fisher Scientific, Madison, WI, USA). For each spectrum, 32 scans were collected at a resolution of 4 cm^{-1} in the range of 400–4500 cm^{-1}.

RM nanoparticles were ball milled (400 rpm for 2 h), dried in an oven (60ºC for 24 h), and dispersed in each of 16 organic solvents and water. In each case, 1.5 mg of RM and 10 mL of solvent were added successively to a glass vial. The dilute concentration was selected to make it easier to detect visually changes in dispersion (Wieneke et al., 2012). The glass vials were shaken manually for 2 min and kept stationary for 4 h. Dispersion stabilities were evaluated visually and photographs were taken. Manual shaking was adopted because transparent dispersions were obtained easily by this method, or otherwise, sedimentation happened

https://doi.org/10.1007/s42860-023-00263-3 Published online by Cambridge University Press

Table 2 The HSPs and Kamlet-Taft's solvatochromic parameters of testing solvents

Solvent No	Solvents	δ_d[a] ($MPa^{1/2}$)	δ_p[a] ($MPa^{1/2}$)	δ_h[a] ($MPa^{1/2}$)	α[b]	β[b]	$\alpha+\beta$	π^*[b]
1	n,n-Dimethyl acetamide	16.8	11.5	10.2	0	0.76	0.76	0.88
2	Dimethyl sulfoxide	18.4	16.4	10.2	0	0.76	0.76	1.00
3	Tetrahydrofuran	16.8	5.7	8.0	0	0.55	0.55	0.58
4	Chloro-benzene	19.0	4.3	2.0	0	0.07	0.07	0.71
5	o-Xylene	17.8	1.0	3.1	0	0.12	0.12	0.43
6	n-Methyl-2-pyrrolidone	18.0	12.3	7.2	0	0.77	0.77	0.92
7	Ethyl benzoate	17.9	6.2	6.0	0	0.41	0.41	0.74
8	Acetonitrile	15.3	18.0	6.1	0.19	0.40	0.59	0.75
9	Styrene	18.6	1.0	4.1	0	0.12	0.12	-
10	Chloroform	17.8	3.1	5.7	0.20	0.10	0.30	0.58
11	1,1,2,2-Tetrachloroethane	18.8	5.1	5.3	0	0	0	0.95
12	n-Heptane	15.3	0	0	0	0	0	0.08
13	Ethanol	15.8	8.8	19.4	0.98	0.66	1.64	0.60
14	t-Butyl alcohol	15.2	5.1	14.7	0.84	0.84	1.68	0.47
15	Diethylene glycol	16.6	12.0	20.7	0.90	0.52	1.42	0.92
16	Ethyl acetate	15.8	5.3	7.2	0	0.45	0.45	0.55
17	Water	15.5	16.0	42.3	1.17	0.47	1.64	1.09

[a] Data from Hansen (2007)

[b] Data from Marcus (1993)

even after ultrasonic agitation (Wang et al., 2013); color changes in aromatic solvents due to degradation were observed during ultrasonic agitation (Wieneke et al., 2012); the dispersion state obtained by this method was sufficient to distinguish good and poor solvents according to measured particle sizes (Alin et al., 2015).

Results and Discussion

Characterization

The measured FTIR spectrum of RM (Fig. 1) matched well with the characteristic infrared absorption of muscovite (Hunt & Turner, 1953; Nahin, 1952; Stubičan & Roy, 1961). The peak at 3621 cm^{-1} was attributed to the stretching of H–O groups and HB with a specific length (Plyusnina & Kapitonova, 1972). The peaks at 3448 and 1637 cm^{-1} were caused by the stretching and bending vibration of H–O groups or water molecules, respectively (Schroeder, 2002; Zhang et al., 2022). The peaks at 1027 cm^{-1} and ~ 500 cm^{-1} (e.g. 475 cm^{-1} and 529 cm^{-1}) corresponded to the stretching and bending

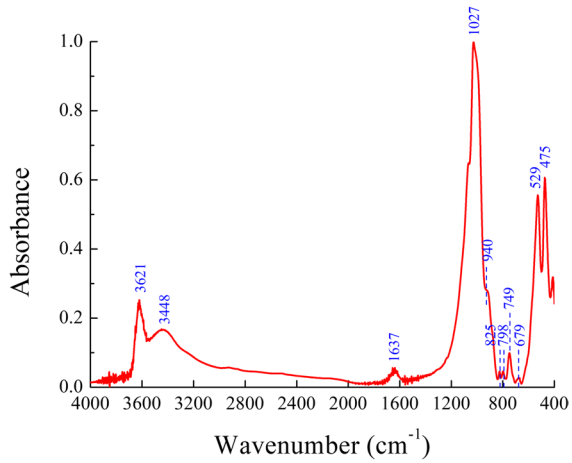

Fig. 1 FTIR spectrum of RM

vibration of Si–O groups, respectively (Beran, 2002). The shoulder peak at 940 cm^{-1} was associated with the stretching vibration of the Al–O group (Beran, 2002; Zhang et al., 2022). The peaks at 679, 749, 798, and 825 cm^{-1} were assigned to the comprehensive effect of the coupling of Al–O and Si–O vibrations, as well

https://doi.org/10.1007/s42860-023-00263-3 Published online by Cambridge University Press

as Si–O–Si and Si–O–Al vibrations (Beran, 2002; Fali et al., 2021).

Determination of a solubility rotated-ellipsoid (SRE)

In this section, the HSPs of a solvent and a solute are denoted as (δ_{d1}, δ_{p1}, δ_{h1}) and (δ_{d2}, δ_{p2}, δ_{h2}), respectively. According to Hansen (1967), the solubility of a solvent was represented by a point located at (δ_{d1}, δ_{p1}, δ_{h1}) in $\delta_d \times \delta_p \times \delta_h$ space, while that of a solute by a solubility region centered at (δ_{d2}, δ_{p2}, δ_{h2}). The solubility region was usually modeled as a sphere, an axis-aligned ellipsoid (the main axes of which were parallel to the δ_d, δ_p, and δ_h axes, respectively), or a rotated-ellipsoid (which was arbitrarily oriented). The rotated-ellipsoid model was adopted in the present study for its advantage in fitting complex shapes of solubility regions (Weng & Wang, 2022).

An optimal SRE of solute was defined as the one which included all good solvents (i.e. solvents for which the solute-affinity was greater than a certain threshold), had the smallest number of outliers (i.e. good solvents that fell outside or poor solvents inside an SRE), and had the smallest volume. It was identified by nine parameters $\mathbf{x}_{rel}=(\delta_{2d}, \delta_{2p}, \delta_{2h}, a, b, c, \theta_d, \theta_p, \theta_h)$, where a, b, and c ($a>b>c$) are the lengths of three semi-axes, θ_d, θ_p, and θ_h (θ_d, θ_p, $\theta_h \in [-\pi, \pi]$) are three inclination angles. The inclination angles were defined as follows: if an SRE rotated sequentially around δ'_h, δ'_p, and δ'_d axes, by $-\theta_h$, $-\theta_p$, and $-\theta_d$, respectively, it reduced to an axis-aligned ellipsoid, the a, b, and c axes of which coincided with δ'_d, δ'_p, and δ'_h axes, respectively, where a $\delta'_d \times \delta'_p \times \delta'_h$ coordinate system is created by shifting the origin of $\delta_d \times \delta_p \times \delta_h$ system to (δ_{2d}, δ_{2p}, δ_{2h}).

The optimal SRE was determined by solving the following optimization problem (Weng & Wang, 2022):

$$\min\ g_G(\mathbf{x}_{rel}) \text{ and } \min\ g_L(\mathbf{x}_{rel}) \tag{3}$$

where g_G and g_L are the global and local searching functions which take the forms of Eqs. 4 and 5, respectively,

$$g_G(\mathbf{x}_{rel}) = 1 - F(\mathbf{x}_{rel}) \tag{4}$$

$$g_L(\mathbf{x}_{rel}) = n_g + n_t + V_{rel}/k \tag{5}$$

where n_t is the total number of outliers, n_g is the number of good-solvent outliers (i.e. good solvents that fell outside an SRE), $V_{rel}=4\pi \cdot a \cdot b \cdot c/3$ is the volume of SRE, k is a constant, F is fitted data calculated by Eqs. 6, 7 (Hansen, 2007)

$$F(\mathbf{x}_{rel}) = \left(\prod_{i=1}^{N} f_i(\mathbf{x}_{rel})\right)^{\frac{1}{N}} \tag{6}$$

$$f_i(\mathbf{x}_{rel}) = \begin{cases} e^{(R_i - Ra_i)}, & s_i = 1, Ra_i > R_i \\ e^{(Ra_i - R_i)}, & s_i = 0, Ra_i < R_i \\ 1, & \text{otherwise} \end{cases} \tag{7}$$

where N is the number of testing solvents, Ra_i is the distance from the HSPs of solute to the HSPs of ith solvent, R_i is the distance from the HSPs of solute to the intersection point of Ra_i and SRE surface, s_i is the solubility of a solute in a solvent measured by experiments, $s_i = 1$ denotes a good solvent and $s_i = 0$ a poor one (i.e. a solvent for which the solute-affinity was lower than a certain threshold), and data fit F reaches the maximum value of 1 when all good solvents lie inside and all poor solvents outside the SRE.

The optimization problem was solved by a hybrid global-local searching algorithm (Weng, 2016), where global and local searching were performed using a restartable particle swarm searching algorithm and a Nelder-Mead simplex algorithm, respectively; local searching was activated when the value of the global objective function was below a threshold. The algorithm recorded abundant local optima, from which the global optimum/optima was/were figured out.

Solubility of RM in solvents

The dispersion of RM in testing solvents after being kept still for 4 h are shown in Fig. 2.

The stabilities of RM-solvent dispersions were classified into three grades according to the morphology of sediments on the bottom of glass vials: (1) no visible sediments in styrene; (2) fine-powdery sediments uniformly covering the vial bottom in chlorobenzene, o-xylene, and chloroform, (3) sediments involving granules or flakes apparently bigger than those in case 2 and/or non-uniformly distributed on the vial bottom in the remaining solvents. The solvents having the best dispersion stabilities of grades

https://doi.org/10.1007/s42860-023-00263-3 Published online by Cambridge University Press

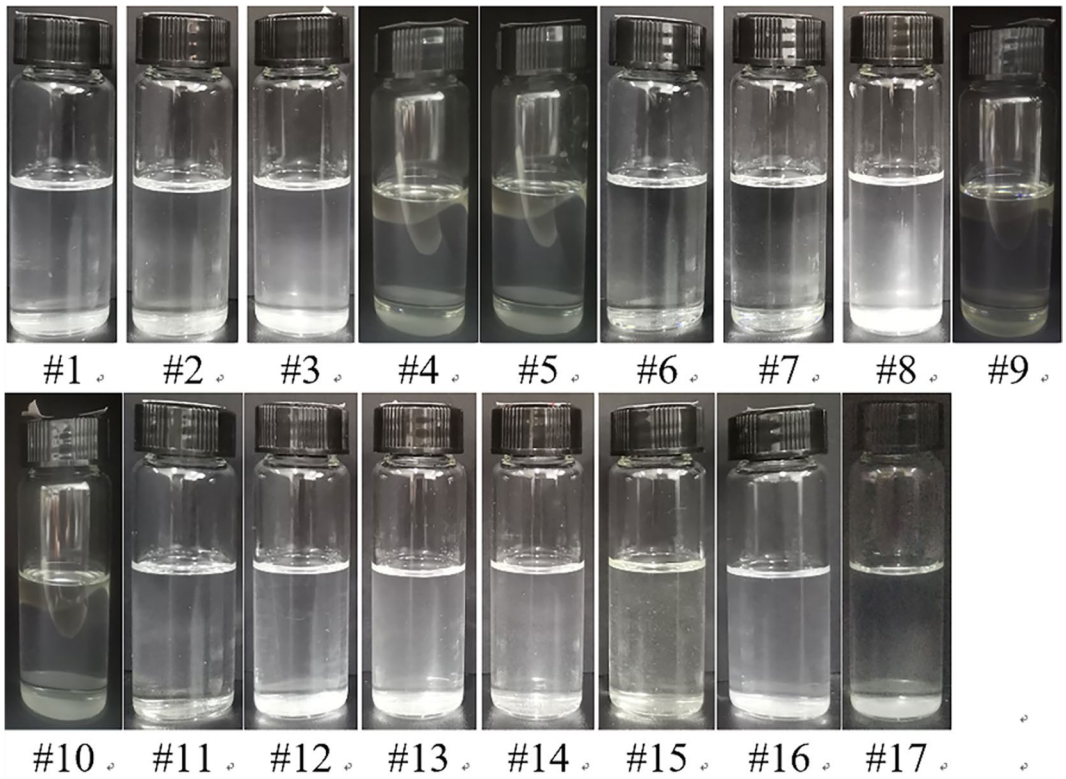

Fig. 2 Dispersion of RM in testing solvents after being kept still for 4 h

(1) and (2) were regarded as good solvents and assigned a RM-solubility s_i value of 1, the solvents having poor dispersion stabilities of grade (3) were taken as poor solvents and assigned a RM-solubility s_i value of 0. The experimental results are given in Table 3.

Computer simulation

The HSPs (Table 2) and measured RM-solubilities s_i (Table 3) of 16 organic solvents were used as input data for calculations. Water was excluded because of its susceptibility to the local environment (Hansen, 2007). Simulation parameters were the same as those reported by Weng and Wang (2022). The output data were the HSPs, total number of outliers, n_t, number of good-solvent outliers, n_g, and relative energy difference (RED) of each solute-solvent pair, i.e. $RED_i = Ra_i/R_i$ ($i = 1, \ldots, N$). A RED value of < 1 denotes a good solute-solvent affinity, > 1 denotes a poor affinity, and $= 1$ denotes a boundary condition.

HSPs and mechanisms of solvent dispersion of RM

The parameter values of the resultant SRE of RM were $\delta_d = 18.301$ MPa$^{1/2}$, $\delta_p = 2.366$ MPa$^{1/2}$, $\delta_h = 3.727$ MPa$^{1/2}$, $a = 2.691$ MPa$^{1/2}$, $b = 2.133$ MPa$^{1/2}$, $c = 0.640$ MPa$^{1/2}$, $\theta_d = 1.257$ rad, $\theta_p = 0.626$ rad, $\theta_h = 1.260$ rad, and a volume of 15.383 MPa$^{3/2}$ (Fig. 3). The total solubility parameter δ_t of RM was 18.826 MPa$^{1/2}$. All good solvents fell inside and all poor solvents outside of the SRE, i.e. $n_t = n_g = 0$, the RED of each RM-solvent pair is given in Table 4.

Compared to the HSPs of hydrophilic raw halloysite (Table 1), the dispersion the HSP component of RM was greater by 1.501 MPa$^{1/2}$, while the polar and HB HSP components of RM were less by 10.234 MPa$^{1/2}$ and 13.673 MPa$^{1/2}$, respectively. In contrast, three good solvents of RM (i.e. chloro-benzene, chloroform, and o-xylene) also had the greatest concentrations of organophilic synthetic mica MTE (modified by a quaternary ammonium ion with trioctyl chain) among the ten testing solvents given by Huth et al. (2018). The difference between the HSPs

https://doi.org/10.1007/s42860-023-00263-3 Published online by Cambridge University Press

Table 3 Stabilities of RM-solvent dispersions and RM-solubilities s_i of the solvents tested

Solvent	Dispersion stability	s_i
n,n-Dimethyl acetamide	–	0
Dimethyl sulfoxide	–	0
Tetrahydrofuran	–	0
Chloro-benzene	+	1
o-Xylene	+	1
n-Methyl-2-pyrrolidone	–	0
Ethyl benzoate	–	0
Acetonitrile	–	0
Styrene	++	1
Chloroform	+	1
1,1,2,2-Tetrachloroethane	–	0
n-Heptane	–	0
Ethanol	–	0
t-Butyl alcohol	–	0
Diethylene glycol	–	0
Ethyl acetate	–	0
Water	–	0

"++" denotes a stable dispersion with no visible sediments, "+" denotes a dispersion with fine-powdery sediments uniformly covering the bottom of the vial, and "–" denotes a dispersion with sediments involving granules or flakes apparently bigger than those in case (b) and/or non-uniformly distributed on vial bottom

calculation proposed here and that suggested by Huth et al. (2018) is that in the former, the algorithm confined the HSPs of RM in a subspace constructed by the HSPs of good solvents (Fig. 3), while in the latter, the HSPs of RM were determined from the HSPs of solvents and a wide range of RM concentrations. To minimize the discrepancy, the HSPs of MTE were recalculated by considering exclusively solvents with the highest MTE concentrations (≥5%), the results obtained were $\delta_d = 18.1$ MPa$^{1/2}$, $\delta_p = 3.3$ MPa$^{1/2}$, $\delta_h = 3.8$ MPa$^{1/2}$. Compared to the recalculated values, the dispersion HSP component of RM was greater by 0.201 MPa$^{1/2}$, while the polar and HB HSP components were smaller by 0.934 MPa$^{1/2}$ and 0.073 MPa$^{1/2}$, respectively. Theoretically, an increase in the number of hydroxyl groups led to an increase in polar and a greater increase in the HB HSP component (Huth et al., 2018). Meanwhile, hydroxyl groups were unique with strong polarity and HB ability on the mica surface. The results revealed, therefore, that RM had fewer surface hydroxyl groups than MTE. The RMs have been recognized to have high hydrophilicity (contact angle of ~10º) (Xue et al., 2018), while synthetic mica was made from talc with relatively low hydrophilicity (contact angle of ~50–60º) (Wang et al., 2009) and the hydroxyl groups within the silicate layer were partially replaced with fluorine (Tateyama et al., 1992). The polar and HB HSP components of RM obtained in the present study, however, were surprisingly smaller than the respective components of MTE, a synthetic mica modified with a surfactant which had hydrophobic hydrogenated tails.

Generally, good solvent-solute affinity could be estimated by high similarities in the respective partial polarities of both phases, which is known as the principle of "like dissolves like." Two polarity scales were considered herein: Hansen's HSP components δ_d, δ_p, and δ_h, denoting the contributions from dispersion, dipole-dipole and dipole-induced-dipole, and HB forces, respectively (Hansen, 1967); Kamlet-Taft's solvatochromic parameters π*, α, and β, denoting the dipolarity/polarizability, HB acidity, and HB basicity of solvents, respectively (Kamlet & Taft, 1976a, 1976b; Kamlet et al., 1977). The low polar, δ_p, and HB, δ_h, HSP components of RM were comparable to the low dipolarity/polarizability, π*, and HB ability, α + β, of the four good solvents (Table 2), which suggested weak polar and HB interactions in good-solvent dispersion. This was because of the limited number of hydroxyl groups present on the RM surface, owing to the low K^+/H^+ exchange ratio in an environment with a small amount of water/moisture (Bowers et al., 2008). The low degree of hydration of RM was evidenced by the weak peaks at 1637 and 3448 cm^{-1} in the FTIR spectrum, which represented the vibrations of H–O groups on RM surface and adsorbed molecular H_2O (Schroeder, 2002). On the contrary, the strong dispersion forces in good-solvent dispersions were indicated by the high dispersion HSP components, δ_d, of both good solvents and RM. Among the poor solvents, water had a relatively low dispersion HSP component, δ_d, of 15.5 MPa$^{1/2}$, a high polar HSP component, δ_p, of 16.0 MPa$^{1/2}$, and the highest HB HSP component, δ_h, of 42.3 MPa$^{1/2}$, or, the strongest dipolarity/polarizability, π*, of 1.09 and HB abilities, α + β, of 1.64. Although RM has the highest hydration level in water, the results revealed that the polar and HB forces generated by the highly hydrated RM were not strong enough to match the

https://doi.org/10.1007/s42860-023-00263-3 Published online by Cambridge University Press

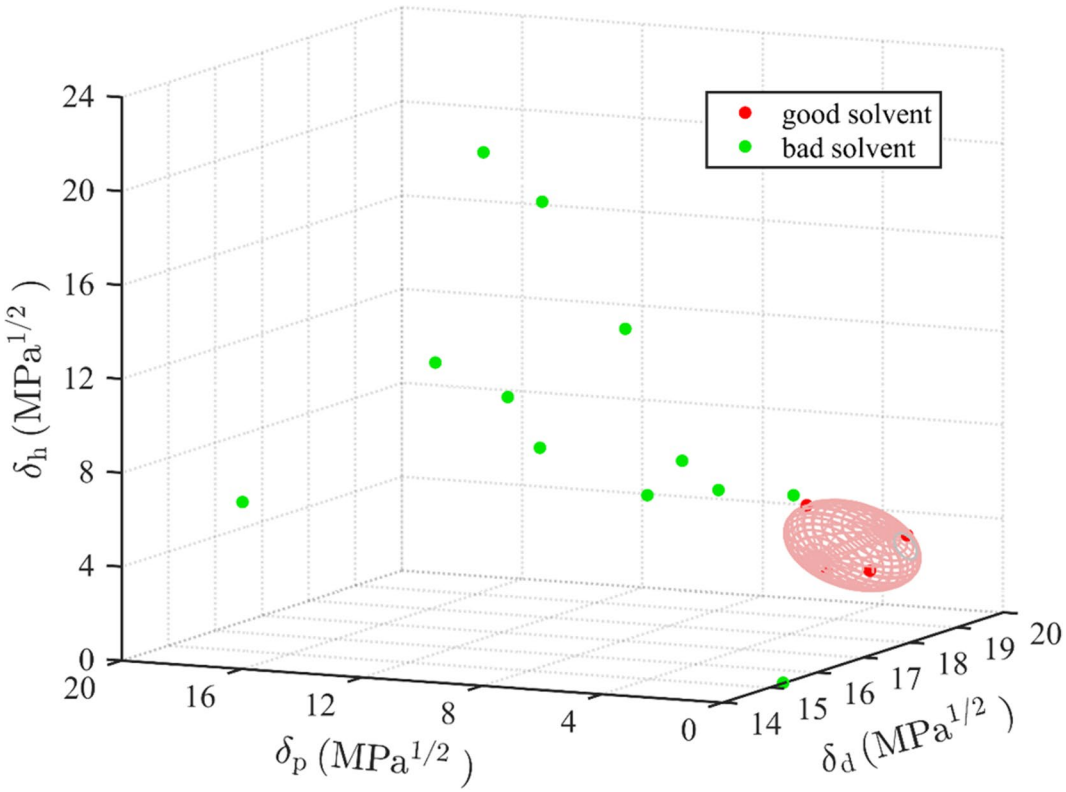

Fig. 3 The SRE of RM

Table 4 The REDs of RM-solvent pairs

Solvents	δ_d[a] (MPa$^{1/2}$)	δ_p[a] (MPa$^{1/2}$)	δ_h[a] (MPa$^{1/2}$)	RED
n,n-Dimethyl acetamide	16.8	11.5	10.2	5.406
Dimethyl sulfoxide	18.4	16.4	10.2	6.961
Tetrahydrofuran	16.8	5.7	8.0	2.875
Chloro-benzene	19.0	4.3	2.0	1.000
o-Xylene	17.8	1.0	3.1	1.000
n-Methyl-2-pyrrolidone	18.0	12.3	7.2	4.760
Ethyl benzoate	17.9	6.2	6.0	2.093
Acetonitrile	15.3	18.0	6.1	9.340
Styrene	18.6	1.0	4.1	1.000
Chloroform	17.8	3.1	5.7	1.000
1,1,2,2-Tetrachloroethane	18.8	5.1	5.3	1.663
n-Heptane	15.3	0	0	5.830
Ethanol	15.8	8.8	19.4	7.988
t-Butyl alcohol	15.2	5.1	14.7	5.367
Diethylene glycol	16.6	12.0	20.7	9.403
Ethyl acetate	15.8	5.3	7.2	3.714

[a] Data from Hansen (2007)

respective molecular forces of solvents. Therefore, low dispersion forces together with the highest possible polar and HB forces generated on the RM-based interface were not sufficient to disperse RM. The other two poor solvents, dimethyl sulfoxide and 1,1,2,2-tetrachloroethane, had the fourth and second highest dispersion HSP components, δ_d, of 18.4 and 18.8 MPa$^{1/2}$, respectively. For dimethyl sulfoxide, its strong polar and HB abilities were represented by a high polar HSP component, δ_p, of 16.4 MPa$^{1/2}$ and high HB HSP component, δ_h, of 10.2 MPa$^{1/2}$, or, a high dipolar/polarization parameter, π*, of 1.00 and high HB basicity, β, of 0.76. For 1,1,2,2-tetrachloroethane, although it had three HSP components closest to those of good solvents, its strong dipolarity/polarization ability was evidenced by a rather high Kamlet-Taft π* value of 0.95. The poor affinity between the two solvents and RM was also represented by their RED values, i.e. 6.961 for dimethyl sulfoxide and 1.663 for 1,1,2,2-tetrachloroethane (Table 4). This revealed that, even in solvents with high dispersion HSP components comparable to that of RM, the unbalanced polar and HB abilities of RM and organic

https://doi.org/10.1007/s42860-023-00263-3 Published online by Cambridge University Press

solvents would also ruin the dispersion. The results indicated that the dispersion behavior of RM in solvents was similar to those of organophilic modified synthetic mica (Huth et al., 2018) and modified Mnt (Ho & Glinka, 2003), but contrary to those of hydrophilic raw halloysite (Zhou et al., 2020) and raw Mnt (Choi et al., 2004).

Conclusions

This study proposed a method for determining the Hansen solubility parameters (HSPs) of raw muscovite (RM). The solubilities of RM in 17 solvents were evaluated according to dispersion states. Experimental results showed that RM was well dispersed in styrene, chloro-benzene, chloroform, and o-xylene. Based on the HSPs of solvents and measured RM solubilities, the HSPs of RM were calculated as the center of the optimal solubility rotated-ellipsoid (SRE) in HSP space, which included all good solvents, had the smallest number of outliers, and had the smallest volume. The derived dispersion, polar, and HB HSP components of RM were 18.301, 2.366, and 3.727 $MPa^{1/2}$, respectively.

By considering the HSPs (δ_d, δ_p, δ_h) and Kamlet-Taft's solvatochromic parameters (π^*, α, β) of solvents, the mechanisms of solvent dispersion of RM were explored. The low polarity of RM was due to the hindered K^+/H^+ exchange on RM surface in an environment with a limited amount of water/moisture. RM was well dispersed in organic solvents with high dispersion HSP components, δ_d, and weak polar, δ_p, and HB, δ_h, HSP components finely tuned to matching the surface property of RM at a specific hydration level.

The HSPs of RM obtained from the dispersion method could only be used to predict/characterize interactions on RM-based interfaces in material fabrication processes with strictly controlled environmental water/moisture content (e.g. in processing of RM/polymer nanocomposites); otherwise, the changes in surface property of RM induced by variant hydration levels should be taken into consideration. The HSP calculation method proposed here was applied to all clay minerals.

Acknowledgements This research was supported by the Public Welfare Technology Application Research Project of Zhejiang Province under Grant no. LGG21E030012.

Data Availability All data are given in the paper and supplementary materials.

Code Availability The codes developed and/or used in the current study are available from the corresponding author on reasonable request.

Declarations

Conflict of Interest The authors declare no conflicts of interest.

References

Alin, J., Rubino, M., & Auras, R. (2015). Effect of the solvent on the size of clay nanoparticles in solution as determined using an ultraviolet–visible (UV-Vis) spectroscopy methodology. *Applied Spectroscopy, 69*(6), 671–678. https://doi.org/10.1366/14-07704

Arias, J. J. R., Rosa, J., & Marques, M. D. F. V. (2019). Influence of phyllosilicate structure on performance of polypropylene nanocomposites prepared via in-situ polymerization. *Journal of Nanoscience and Nanotechnology, 19*(4), 1908–1922. https://doi.org/10.1166/jnn.2019.16339

Asgari, M., & Sundararaj, U. (2018). Silane functionalization of sodium montmorillonite nanoclay: The effect of dispersing media on intercalation and chemical grafting. *Applied Clay Science, 153*, 228–238. https://doi.org/10.1016/j.clay.2017.12.020

Beran, A. (2002). Infrared spectroscopy of micas. *Reviews in Mineralogy and Geochemistry, 46*(1), 351–369. https://doi.org/10.2138/rmg.2002.46.07

Bowers, G. M., Bish, D. L., & Kirkpatrick, R. J. (2008). Cation exchange at the mineral-water interface: H3O+/K+ competition at the surface of nano-muscovite. *Langmuir, 24*(18), 10240–10244. https://doi.org/10.1021/la8021112

Choi, Y. S., Ham, H. T., & Chung, I. J. (2004). Effect of monomers on the basal spacing of sodium montmorillonite and the structures of polymer-clay nanocomposites. *Chemistry of Materials, 16*(13), 2522–2529. https://doi.org/10.1021/cm0348601

Fali, A., Gamage, S., Howard, M., Folland, T. G., Mahadik, N. A., Tiwald, T., Bolotin, K., Caldwell, J. D., & Abate, Y. (2021). Nanoscale spectroscopy of dielectric properties of mica. *ACS Photonics, 8*(1), 175–181. https://doi.org/10.1021/acsphotonics.0c00951

Hansen, C. M. (2007). *Hansen solubility parameters: A user's handbook* (2nd ed.). CRC Press.

Hansen, C. M. (1967). The three dimensional solubility parameter and solvent diffusion coefficient, their importance in surface coating formulation. Doctoral dissertation, Danish Technical Press, Copenhagen.

Hildebrand, J. H. (1949). A critique of the theory of solubility of non-electrolytes. *Chemical Review, 44*(1), 37–45. https://doi.org/10.1021/cr60137a003

Ho, D. L., & Glinka, C. J. (2003). Effects of solvent solubility parameters on organoclay dispersions. *Chemistry of Materials, 15*(6), 1309–1312. https://doi.org/10.1021/cm021717194

Hojiyev, R., Ulcay, Y., & Çelik, M. S. (2017). Development of a clay-polymer compatibility approach for nanocomposite applications. *Applied Clay Science, 146*, 548–556. https://doi.org/10.1016/j.clay.2017.07.007

Hunt, J. M., & Turner, D. S. (1953). Determination of mineral constituents of rocks by infrared spectroscopy. *Analytical Chemistry, 25*(8), 1169–1174. https://doi.org/10.1021/ac60080a007

Huth, M., Chen, C. W., & Wagner, V. (2018). Measurement of Hansen solubility parameters for organophilic fluoromica and evaluation of potential solvents for exfoliation. *Applied Clay Science, 155*, 120–125. https://doi.org/10.1016/j.clay.2018.01.012

Kamlet, M. J., & Taft, R. W. (1976). The solvatochromic compoarison method. 1. The β-scale of solvent hydrogen-bond acceptor (HBA) basicities. *Journal of the American Chemical Society, 98*(2), 377–383. https://doi.org/10.1021/ja00418a009

Kamlet, M. J., & Taft, R. W. (1976). The solvatochromic comparison method. 2. The α-scale of solvent hydrogen-bond donor (HBD) acidities. *Journal of the American Chemical Society, 98*(10), 2886–2894. https://doi.org/10.1021/ja00426a036

Kamlet, M. J., Abboud, J. L., & Taft, R. W. (1977). The solvatochromic comparison method. 6. The π* scale of solvent polarities. *Journal of the American Chemical Society, 99*(18), 6027–6038. https://doi.org/10.1021/ja00460a031

Li, L., Jiang, Z., Xu, J., & Fang, T. (2014). Predicting poly(vinyl pyrrolidone)'s solubility parameter and systematic investigation of the parameters of electrospinning with response surface methodology. *Journal of Applied Polymer Science, 131*(11), 40304. https://doi.org/10.1002/app.40304

Lu, J., Hong, C. K., & Wool, R. P. (2004). Bio-based nanocomposites from functionalized plant oils and layered silicate. *Journal of Polymer Science: Part b: Polymer Physics, 42*(8), 1441–1450. https://doi.org/10.1002/polb.20027

Marcus, Y. (1993). The properties of organic liquids that are relevant to their use as solvating solvents. *Chemical Society Reviews, 22*(6), 409–416. https://doi.org/10.1039/CS9932200409

Mohammadi, H., & Moghbeli, M. R. (2018). Organically modified-grafted mica (OMGM) nanoparticles for reinforcement of polypropylene. *Iranian Polymer Journal, 27*(2), 125–135. https://doi.org/10.1007/s13726-017-0593-2

Nahin, P. G. (1952). Infra-red analysis of clay and related minerals. *Clays and Clay Minerals, 1*, 112–118. https://doi.org/10.1346/CCMN.1952.0010115

Pauling, L. (1930). The structure of the micas and related minerals. *Proceedings of the National Academy of Sciences of the United States of America, 16*(2), 123–129. https://doi.org/10.1073/pnas.16.2.123

Plyusnina, I. I., & Kapitonova, T. A. (1972). Infrared absorption spectra of micas in the on stretching region. *Journal of Applied Spectroscopy, 16*(3), 351–353. https://doi.org/10.1007/BF00625559

Qin, J. W., Wang, X., Jiang, Q. W., & Cao, M. H. (2019). Optimizing dispersion, exfoliation, synthesis, and device fabrication of inorganic nanomaterials using Hansen solubility parameters. *ChemPhysChem, 20*(9), 1069–1097. https://doi.org/10.1002/cphc.201900110

Schroeder, P. A. (2002). Infrared spectroscopy in clay science. In CMS workshop lectures, vol. 11, Teaching clay science, Rule, A. & Guggenheim, S. eds., The Clay Mineral Society, Aurora, USA.

Stubičan, V., & Roy, R. (1961). Isomorphous substitution and infra-red spectra of the layer lattice silicates. *American Mineralogist, 46*(1–2), 32–51.

Tateyama, H., Nishimura, S., Tsunematsu, K., Jinnai, K., Adachi, Y., & Kimura, M. (1992). Synthesis of expandable fluorine mica from talc. *Clays and Clay Minerals, 40*(2), 180–185. https://doi.org/10.1346/CCMN.1992.0400207

Wang, J. W., Kalinichev, A. G., & Kirkpatrick, R. J. (2009). Asymmetric Hydrogen bonding and orientational ordering of water at hydrophobic and hydrophilic surfaces: A comparison of water/vapor, water/talc, and water/mica interfaces. *Journal of Physical Chemistry C, 113*(25), 11077–11085. https://doi.org/10.1021/jp9018316

Wang, S. H., Liu, J. H., Pai, C. T., Chen, C. W., Chung, P. T., Chiang, A. S. T., & Chang, S. J. (2013). Hansen solubility parameter analysis on the dispersion of zirconia nanocrystals. *Journal of Colloid and Interface Science, 407*, 140–147. https://doi.org/10.1016/j.jcis.2013.07.001

Weng, M. (2016). Determination of the Hansen solubility parameters with a novel optimization method. *Journal of Applied Polymer Science, 133*(16), 43328. https://doi.org/10.1002/app.43328

Weng, M., & Wang, X. H. (2022). Determining Hansen solubility parameters by a rotated ellipsoid-based method. *Polymer Science, Series A: Polymer Physics, 64*(6), 591–600. https://doi.org/10.1134/S0965545X22700390

Wieneke, J. U., Kommoß, B., Gaer, O., Prykhodko, I., & Ulbricht, M. (2012). Systematic investigation of dispersions of unmodified inorganic nanoparticles in organic solvents with focus on the Hansen solubility parameters. *Industrial & Engineering Chemistry Research, 51*(1), 327–334. https://doi.org/10.1021/ie201973u

Xue, X. P., Xu, Z. H., Pedruzzi, I., Ping, L., & Yu, J. G. (2018). Interaction between low molecular weight carboxylic acids and muscovite: Molecular dynamic simulation and experiment study. *Colloids and Surfaces A: Physicochemical and Engineering Aspects, 559*, 8–17. https://doi.org/10.1016/j.colsurfa.2018.09.033

Yen, M., Bitla, Y., & Chu, Y. H. (2019). van der Waals heteroepitaxy on muscovite. *Materials Chemistry and Physics, 234*, 185–195. https://doi.org/10.1016/j.matchemphys.2019.05.053

Zhang, D. Y., Li, C. C., Lin, N. Z., Xie, B. S., & Chen, J. (2022). Mica-stabilized polyethylene glycol composite phase change materials for thermal energy storage. *International Journal of Minerals, Metallurgy and Materials, 29*(1), 168–176. https://doi.org/10.1007/s12613-021-2357-4

Zhao, Z. N., Li, Y. H. W., Lei, W., & Hao, Q. L. (2022). Modified graphene/muscovite nanocomposite as a lubricant additive: Tribological performance and mechanism. *Lubricants, 10*(8), 190. https://doi.org/10.3390/lubricants10080190

Zhong, G. K., & Li, J. Y. (2020). Muscovite mica as platform for flexible electronics. *Journal of Materiomics, 6*(2), 455–457. https://doi.org/10.1016/j.jmat.2019.12.004

Zhou, Z. Y., Fang, L. Z., Cao, Y. X., Wang, W. J., Wang, J. F., Yang, Y. Y., & Liu, Y. K. (2020). Determination of

Hansen solubility parameters of halloysite nanotubes and prediction of its compatibility with polyethylene oxide. *Colloids and Surfaces A: Physicochemical and Engineering Aspects, 601*, 125031. https://doi.org/10.1016/j.colsurfa.2020.125031

https://doi.org/10.1007/s42860-023-00263-3 Published online by Cambridge University Press